ARMY RESEARCH LABORATORY

Finite Strain Analysis of Shock Compression of Brittle Solids Applied to Titanium Diboride

by John D Clayton

ARL-RP-0495 **July 2014**

**A reprint from the *International Journal of Impact Engineering*,
Vol. 73, pp. 56–65, 2014.**

NOTICES

Disclaimers

The findings in this report are not to be construed as an official Department of the Army position unless so designated by other authorized documents.

Citation of manufacturer's or trade names does not constitute an official endorsement or approval of the use thereof.

Destroy this report when it is no longer needed. Do not return it to the originator.

Army Research Laboratory
Aberdeen Proving Ground, MD 21005-5069

ARL-RP-0495 **July 2014**

Finite Strain Analysis of Shock Compression of Brittle Solids Applied to Titanium Diboride

John D Clayton
Weapons and Materials Research Directorate, ARL

A reprint from the *International Journal of Impact Engineering,*
Vol. 73, pp. 56–65, 2014.

REPORT DOCUMENTATION PAGE	Form Approved OMB No. 0704-0188

1. REPORT DATE *(DD-MM-YYYY)*	2. REPORT TYPE	3. DATES COVERED (From - To)
July 2014	Reprint	July 2013–July 2014

4. TITLE AND SUBTITLE
Finite Strain Analysis of Shock Compression of Brittle Solids Applied to Titanium Diboride

5a. CONTRACT NUMBER

5b. GRANT NUMBER

5c. PROGRAM ELEMENT NUMBER

6. AUTHOR(S)
John D Clayton

5d. PROJECT NUMBER
DRI13-WMR-019

5e. TASK NUMBER

5f. WORK UNIT NUMBER

7. PERFORMING ORGANIZATION NAME(S) AND ADDRESS(ES)
U.S. Army Research Laboratory
ATTN: RDRL-WMP-C
Aberdeen Proving Ground, MD 21005-5069

8. PERFORMING ORGANIZATION REPORT NUMBER
ARL-RP-0495

9. SPONSORING/MONITORING AGENCY NAME(S) AND ADDRESS(ES)

10. SPONSOR/MONITOR'S ACRONYM(S)

11. SPONSOR/MONITOR'S REPORT NUMBER(S)

12. DISTRIBUTION/AVAILABILITY STATEMENT
Approved for public release; distribution is unlimited.

13. SUPPLEMENTARY NOTES
A reprint from the *International Journal of Impact Engineering*, Vol. 73, pp. 56–65, 2014.

14. ABSTRACT
A finite strain theory is developed for polycrystalline brittle materials undergoing shock loading. Inelastic deformation arises principally from extension and opening or sliding of microcracks, and depends on pressure as well as deviatoric stress. In the general theory, internal energy depends on a logarithmic measure of finite elastic strain, entropy, and an internal variable associated with fracture. The theory is applied towards planar shock loading of an isotropic sample under possible static pre-stress. An exact analytical solution is derived when inelasticity is idealized as rate independent. The model and solution are applied to describe polycrystalline ceramic titanium diboride. Results provide new insight into experimental shock data, demonstrating importance of elastic nonlinearity and pressure dependent strength. The model describes shock pressure, mean stress, and shear stress in shocked titanium diboride, including the double yield point, with a minimal number of fitting parameters. The analysis predicts an increase in the Hugoniot elastic limit and suppression of inelasticity with increasing compressive pre-stress, in agreement with recent experiments.

15. SUBJECT TERMS
ceramics, shock compression, titanium diboride, elasticity, fracture

16. SECURITY CLASSIFICATION OF:			17. LIMITATION OF ABSTRACT	18. NUMBER OF PAGES	19a. NAME OF RESPONSIBLE PERSON
a. REPORT	b. ABSTRACT	c. THIS PAGE			John D Clayton
Unclassified	Unclassified	Unclassified	UU	16	19b. TELEPHONE NUMBER (*Include area code*) (410) 278-6146

Standard Form 298 (Rev. 8/98)
Prescribed by ANSI Std. Z39.18

International Journal of Impact Engineering 73 (2014) 56–65

Contents lists available at ScienceDirect

International Journal of Impact Engineering

journal homepage: www.elsevier.com/locate/ijimpeng

Finite strain analysis of shock compression of brittle solids applied to titanium diboride

J.D. Clayton

Impact Physics, RDRL-WMP-C, US Army Research Laboratory, Aberdeen Proving Ground, MD 21005-5066, USA

ARTICLE INFO

Article history:
Received 24 February 2014
Received in revised form
1 June 2014
Accepted 2 June 2014
Available online 12 June 2014

Keywords:
Ceramics
Shock physics
Plasticity
Damage
Finite strain

ABSTRACT

A finite strain theory is developed for polycrystalline brittle materials undergoing shock loading. Inelastic deformation arises principally from extension and opening or sliding of microcracks, and depends on pressure as well as deviatoric stress. In the general theory, internal energy depends on a logarithmic measure of finite elastic strain, entropy, and an internal variable associated with fracture. The theory is applied towards planar shock loading of an isotropic sample under possible static pre-stress. An exact analytical solution is derived when inelasticity is idealized as rate independent. The model and solution are applied to describe polycrystalline ceramic titanium diboride. Results provide new insight into experimental shock data, demonstrating importance of elastic nonlinearity and pressure dependent strength. The model describes shock pressure, mean stress, and shear stress in shocked titanium diboride, including the double yield point, with a minimal number of fitting parameters. The analysis predicts an increase in the Hugoniot elastic limit and suppression of inelasticity with increasing compressive pre-stress, in agreement with recent experiments.

Published by Elsevier Ltd.

1. Introduction

Brittle solids such as ceramics, rocks, minerals, and glasses demonstrate a variety of deformation mechanisms when subjected to shock loading at stress levels above their Hugoniot Elastic Limit (HEL, i.e., yield strength under planar shock compression). In crystalline materials, these mechanisms can include intergranular fracture, transgranular fracture, pore collapse, dislocation glide, stacking fault propagation, twinning, phase transformations, and shear localization. Brittle materials are informally distinguished from ductile solids such as metals by their increased tendency to fracture rather than deform plastically by slip or twinning. Bonding tends to be covalent or ionic in character, and though exceptions exist, brittle solids tend to have a relatively large ratio of shear to bulk modulus (small Poisson's ratio) in comparison to ductile solids [1].

In the context of dynamic loading, engineering ceramics tend to have a large HEL and small spall strength relative to engineering metals. In brittle solids, dynamic yield strength also tends to depend more strongly on pressure [2,3]. Physically, such pressure dependence results from frictional resistance to crack sliding and resistance to dilatation with pressure that accompanies such sliding. Pressure dependence of strength varies among brittle solids with different compositions and microstructures [4,5]. As shock pressure increases beyond the HEL, shear strength may increase, decrease, or remain constant depending on the material [6], but spall strength more often degrades as cracking increases with increasing shock pressure [4,7], in the limit the pulverized material having zero tensile strength. In contrast, in ductile solids deforming by dislocation-based slip, the dependence of shear strength on pressure is normally small (e.g., Peierls barrier depending on pressure through the shear modulus [8]), as is the dependence of spall strength on impact stress, though again exceptions are possible.

The first part of this paper (§2) develops a finite strain model for brittle solids. A multiplicative decomposition of the deformation gradient is used, wherein inelastic deformation arises primarily from micro-cracks, though contributions from other mechanisms such as dislocation motion are not excluded. This geometrically nonlinear approach parallels that of finite elastic–plastic theory typically used for ductile solids [8–10] and differs from rate-type approaches more often encountered for computational modeling of brittle solids under dynamic loading [11–13]. The present work focuses on an internal energy-based thermodynamic formulation, with internal energy depending on entropy, an internal state variable accounting for damage or defects, and a logarithmic measure

E-mail address: john.d.clayton1.civ@mail.mil.

http://dx.doi.org/10.1016/j.ijimpeng.2014.06.003
0734-743X/Published by Elsevier Ltd.

of thermoelastic strain (specifically, the logarithm of the right thermoelastic stretch tensor).

A few prior works have used the multiplicative decomposition to describe fracture processes in brittle solids [14,15], but these focused on free energy rather than internal energy, and used Green elastic strain rather than logarithmic strain. The latter strain proves more convenient for analysis of planar shocks in isotropic solids, which is undertaken in the second part of this paper (§3). Analysis here follows previous works dealing with elastic–plastic metals [16,17], the primary difference being that in brittle solids, pressure dependent yield strength is considered, which complicates the solution. In this work, it is shown how the Rankine-Hugoniot conditions and the constitutive equations for pressure and shear strength can be reduced to a set of coupled algebraic equations that can be solved for the material state downstream of the shock, given the upstream state and one input variable describing the downstream state (e.g., specific volume or shock pressure). Pre-stress in the material, prior to shock compression, is also newly considered in the present analysis.

In the third part of this paper (§4), model parameters are populated for titanium diboride (TiB_2) and solutions are generated for the shock problem, to axial shock stresses on the order of 50 GPa. Titanium diboride is a strong ceramic whose grains have hexagonal crystal structure. Under impact loading, fracture is thought to be the dominant source of inelasticity [4,6,7], though pore collapse [5] and dislocation motion [18,19] may take place at high pressures. Multiple investigations have discovered that titanium diboride demonstrates a rather unique "double yield", which can be inferred from inflection points in the particle velocity history [5,20–22]. Values of the HEL, and associated physical mechanisms, can vary substantially with microstructure (grain size, porosity, impurities, etc. [5]), which in turn depends on processing route. Spall strength degrades rapidly in the material when shocked above the HEL, providing indirect evidence that fracture is the source of initial yield [4,7].

Key new contributions of the present paper, in the context of prior work, are summarized as follows. The constitutive model and analytical solution consider brittle ceramics with pressure dependent strength, in contrast to [16,17] focused on ductile metals with pressure independent yield. In contrast to [23], which modeled anisotropic single crystals using logarithmic theory, the present work considers isotropic polycrystals (for which some algebra simplifies considerably) with possible lateral pre-stress, with the latter condition not analyzed previously. Furthermore, the current particular application to titanium diboride, which demonstrates the aforementioned unusual double yield mechanism, is also a new contribution.

Notation of continuum physics is used: vectors and tensors are generally written in bold italic, with $(\cdot)^T$, $(\cdot)^{-1}$, and $(\cdot)^{-T}$ denoting transposition, inversion, and the inverse-transpose. Individual components of vectors and tensors are referred to a Cartesian frame and are written in plain italic, with summation over repeated indices. The scalar product of two second-order tensors is $\boldsymbol{A}:\boldsymbol{B} = A_{ij}B_{ij}$.

2. Finite deformation theory

General theory is developed in §2.1. This theory is specialized to isotropic thermoelastic response in §2.2.

2.1. General theory

Let $\boldsymbol{x} = \boldsymbol{x}(\boldsymbol{X},t)$ denote spatial coordinates, at time t, of a material particle with reference coordinates $\boldsymbol{X}$. Assuming $\boldsymbol{x}$ is differentiable, the deformation gradient is

$$\boldsymbol{F} = \nabla_0 \boldsymbol{x} = \boldsymbol{F}^E \boldsymbol{F}^D, \tag{2.1}$$

where ∇_0 denotes the referential gradient (e.g., in Cartesian coordinates, $F_{iJ} = \partial_J x_i = \partial x_i/\partial X_J$) and $\boldsymbol{F}^E$ and $\boldsymbol{F}^D$ denote deformation "gradient" mappings associated with thermoelasticity and defects (e.g., cracks, dislocations, etc.), though neither of the latter generally anholonomic mappings [24] need be compatible (i.e., a true gradient of a vector field). Each is, however, presumed to have positive determinant. In the absence of discontinuities, body forces, and heat sources/conduction, the usual local balance laws of continuum mechanics are [8]

$$\rho_0 = \rho J, \quad \nabla\cdot\boldsymbol{\sigma} = \rho\dot{\boldsymbol{v}}, \quad \boldsymbol{\sigma} = \boldsymbol{\sigma}^T, \quad \dot{U} = \boldsymbol{\sigma} : \nabla\boldsymbol{v}, \quad \rho_0\theta\dot{\eta} \geq 0. \tag{2.2}$$

Reference and spatial mass densities are ρ_0 and ρ, volume ratio is $J = \det\boldsymbol{F}$, Cauchy stress is $\boldsymbol{\sigma}$, particle velocity is $\boldsymbol{v} = \dot{\boldsymbol{x}}$, internal energy per unit reference volume is U, absolute temperature is θ, and entropy per unit reference volume is η. The spatial gradient is ∇ [i.e., $\nabla_k(\cdot) = \partial_k(\cdot) = \partial(\cdot)/\partial x_k$], and time derivatives are taken at fixed $\boldsymbol{X}$. Helmholtz free energy density is $\Psi = U - \theta\eta$.

Applying the polar decomposition to thermoelastic deformation,

$$\boldsymbol{F}^E = \boldsymbol{R}^E\boldsymbol{U}^E = \boldsymbol{V}^E\boldsymbol{R}^E, \quad \boldsymbol{C}^E = \boldsymbol{F}^{ET}\boldsymbol{F}^E = \boldsymbol{U}^{E2}, \quad \boldsymbol{R}^{E-1} = \boldsymbol{R}^{ET}. \tag{2.3}$$

Several thermoelastic strain measures are defined for later use:

$$\boldsymbol{E}^E = \frac{1}{2}\left(\boldsymbol{C}^E - \boldsymbol{1}\right), \quad \boldsymbol{e}^E = \ln\boldsymbol{U}^E = \frac{1}{2}\ln\boldsymbol{C}^E, \quad \boldsymbol{\varepsilon}^E = \ln\boldsymbol{V}^E. \tag{2.4}$$

Definitions and identities for the logarithm of a tensor are discussed in Ref. [25]. Thermoelastic volume change is

$$J^E = \det\boldsymbol{F}^E = \det\boldsymbol{U}^E = \det\boldsymbol{V}^E = \det\left[2\boldsymbol{E}^E + 1\right]^{1/2} = \exp\left(\mathrm{tr}\boldsymbol{e}^E\right) = \exp\left(\mathrm{tr}\boldsymbol{\varepsilon}^E\right). \tag{2.5}$$

Denote by ξ a generic internal state variable associated with evolution of microstructure, e.g., accumulated cracks, voids, or dislocations in the material. Here, ξ is assumed a scalar, but generalization to higher-order tensors and/or multiple state variables poses no difficulties. Assuming uniform properties in the reference state, internal energy density is of the general forms

$$U = U\left(\boldsymbol{F}^E,\eta,\xi\right) = \overline{U}\left(\boldsymbol{E}^E,\eta,\xi\right) = \check{U}\left(\boldsymbol{e}^E,\eta,\xi\right). \tag{2.6}$$

Form $\overline{U}$, incorporating elastic Green strain $\boldsymbol{E}^E$, is the traditional choice for elastic and elastic–plastic crystals [8,9,26,27]. Form $\check{U}$ has been rarely used for anisotropic solids, two exceptions being the analysis of higher-order elastic moduli in Ref. [28] and a recent study of shock compression of sapphire, diamond, and quartz single crystals in Ref. [23]. Define thermodynamic conjugate forces as

$$\overline{\boldsymbol{S}} = \partial\overline{U}/\partial\boldsymbol{E}^E, \quad \check{\boldsymbol{S}} = \partial\check{U}/\partial\boldsymbol{e}^E, \quad \zeta = -\partial\overline{U}/\partial\xi = -\partial\check{U}/\partial\xi. \tag{2.7}$$

Using (2.2) and considering admissible thermomechanical processes, the following constitutive laws can be derived consistently with the first and second laws of thermodynamics (see e.g. Ref. [8]):

$$\boldsymbol{\sigma} = J^{E-1}\boldsymbol{F}^E\overline{\boldsymbol{S}}\boldsymbol{F}^{ET} = J^{E-1}\boldsymbol{F}^E\left(\check{\boldsymbol{S}} : \boldsymbol{M}\right)\boldsymbol{F}^{ET}, \quad \theta = \partial\overline{U}/\partial\eta = \partial\check{U}/\partial\eta;$$
$$J\boldsymbol{\sigma} : \left(\boldsymbol{F}^E\dot{\boldsymbol{F}}^D\boldsymbol{F}^{-1}\right) + \zeta\dot{\xi} \geq 0. \tag{2.8}$$

In the hyperelastic law in the first of (2.8), the following fourth-order tensor is used [25]:

$$\boldsymbol{M}=\frac{\partial \ln \boldsymbol{C}^E}{\partial \boldsymbol{C}^E}=\sum_{i=1}^{3}\frac{1}{\Lambda_i^E}\boldsymbol{P}_i\boxtimes\boldsymbol{P}_i^T+\sum_{i=1}^{3}\sum_{j=1;j\neq i}^{3}\frac{\ln\Lambda_i^E-\ln\Lambda_j^E}{\Lambda_i^E-\Lambda_j^E}\boldsymbol{P}_i\boxtimes\boldsymbol{P}_i^T. \tag{2.9}$$

Here $\Lambda_i^E=(\lambda_i^E)^2$ are the principal values of $\boldsymbol{C}^E$, $(\boldsymbol{A}\boxtimes\boldsymbol{B})_{IJKL}=A_{IK}B_{JL}$, and

$$\boldsymbol{P}_i=\prod_{j=1;j\neq i}^{3}\left(\boldsymbol{C}^E-\Lambda_j^E\boldsymbol{1}\right)\Big/\left(\Lambda_i^E-\Lambda_j^E\right). \tag{2.10}$$

Noting that principal stretches λ_i^E are eigenvalues of $\boldsymbol{U}^E$ (and $\boldsymbol{V}^E$),

$$\boldsymbol{e}^E=\sum_{i=1}^{3}\boldsymbol{P}_i\ln\lambda_i^E=\frac{1}{2}\sum_{i=1}^{3}\boldsymbol{P}_i\ln\Lambda_i^E. \tag{2.11}$$

Defining specific heat at constant strain as $c=\partial U/\partial\theta=-\theta\partial^2\Psi/\partial\theta^2$, the balance of energy becomes

$$\begin{aligned}c\dot{\theta}&=J\boldsymbol{\sigma}:\left(\boldsymbol{F}^E\dot{\boldsymbol{F}}^D\boldsymbol{F}^{-1}\right)+\theta\left(\partial\overline{\boldsymbol{S}}\Big/\partial\theta\right):\dot{\boldsymbol{E}}^E+[\zeta-\theta(\partial\zeta/\partial\theta)]\dot{\xi}\\&=J\boldsymbol{\sigma}:\left(\boldsymbol{F}^E\dot{\boldsymbol{F}}^D\boldsymbol{F}^{-1}\right)+\theta\left(\partial\check{\boldsymbol{S}}\Big/\partial\theta\right):\dot{\boldsymbol{e}}^E+[\zeta-\theta(\partial\zeta/\partial\theta)]\dot{\xi}.\end{aligned} \tag{2.12}$$

Generic kinetic equations for inelasticity are of the state dependent form

$$\dot{\boldsymbol{F}}^D=\dot{\boldsymbol{F}}^D\left(\boldsymbol{F}^E,\eta,\xi\right),\quad \dot{\xi}=\dot{\xi}\left(\boldsymbol{F}^E,\eta,\zeta\right). \tag{2.13}$$

Let U_0 denote internal energy in the elastically unstrained reference state defined by $(\boldsymbol{E}^E,\eta)=(0,\eta_0)$, $(\boldsymbol{e}^E,\eta)=(0,\eta_0)$, and entropy change from this reference state is $\Delta\eta=\eta-\eta_0$. Temperature change from this reference state is $\Delta\theta=\theta-\theta_0$. Let Greek subscripts denote Voigt notation for symmetric indices, e.g., $(\cdot)_{IJ}=(\cdot)_{JI}\leftrightarrow(\cdot)_\alpha$:

$$\begin{aligned}&11\leftrightarrow1,\quad 22\leftrightarrow2,\quad 33\leftrightarrow3,\quad 23=32\leftrightarrow4,\quad 13=31\leftrightarrow5,\\&12=21\leftrightarrow6.\end{aligned} \tag{2.14}$$

The following Taylor series expansions of internal energy are used:

$$\overline{U}=U_0+\overline{C}_\alpha^\eta E_\alpha^E+\frac{1}{2!}\overline{C}_{\alpha\beta}E_\alpha^EE_\beta^E+\frac{1}{3!}\overline{C}_{\alpha\beta\gamma}E_\alpha^EE_\beta^EE_\gamma^E-\theta_0\left[\overline{\Gamma}_\alpha E_\alpha^E\Delta\eta-h(\eta)\right]+f(\xi), \tag{2.15}$$

$$\check{U}=U_0+\check{C}_\alpha e_\alpha^E+\frac{1}{2!}\check{C}_{\alpha\beta}e_\alpha^Ee_\beta^E+\frac{1}{3!}\check{C}_{\alpha\beta\gamma}e_\alpha^Ee_\beta^Ee_\gamma^E-\theta_0\left[\check{\Gamma}_\alpha e_\alpha^E\Delta\eta-h(\eta)\right]+f(\xi). \tag{2.16}$$

Material coefficients evaluated at the unstressed reference state are

$$U_0=\overline{U}(\boldsymbol{0},\eta_0),\quad \overline{C}_\alpha=\left(\partial\overline{U}/\partial E_\alpha^E\right)\big|_0=0; \tag{2.17}$$

$$\overline{C}_{\alpha\beta}=\left(\frac{\partial^2\overline{U}}{\partial E_\alpha^E\partial E_\beta^E}\right)\Big|_0,\quad \overline{C}_{\alpha\beta\gamma}=\left(\frac{\partial^3\overline{U}}{\partial E_\alpha^E\partial E_\beta^E\partial E_\gamma^E}\right)\Big|_0; \tag{2.18}$$

$$\theta_0\overline{\Gamma}_\alpha=\left(\frac{\theta}{c}\frac{\partial\eta}{\partial E_\alpha^E}\right)\Big|_0=-\left(\frac{\partial\theta}{\partial E_\alpha^E}\right)\Big|_0=-\left(\frac{\partial^2\overline{U}}{\partial\eta\partial E_\alpha^E}\right)\Big|_0; \tag{2.19}$$

and

$$U_0=\check{U}(\boldsymbol{0},\eta_0),\quad \check{C}_\alpha=\left(\partial\check{U}/\partial e_\alpha^E\right)\big|_0=0; \tag{2.20}$$

$$\check{U}_{\alpha\beta}=\left(\frac{\partial^2\check{U}}{\partial e_\alpha^E\partial e_\beta^E}\right)\Big|_0,\quad \check{C}_{\alpha\beta\gamma}=\left(\frac{\partial^3\check{U}}{\partial e_\alpha^E\partial e_\beta^E\partial e_\gamma^E}\right)\Big|_0; \tag{2.21}$$

$$\theta_0\check{\Gamma}_\alpha=\left(\frac{\theta}{c}\frac{\partial\eta}{\partial e_\alpha^E}\right)\Big|_0=-\left(\frac{\partial\theta}{\partial e_\alpha^E}\right)\Big|_0=-\left(\frac{\partial^2\check{C}}{\partial\eta\partial e_\alpha^E}\right)\Big|_0. \tag{2.22}$$

Letting $c_0=(\partial U/\partial\theta)\big|_0$ denote a constant specific heat for the unstrained material, the strictly entropic contribution to internal energy is [29]

$$h=c_0[\exp(\Delta\eta/c_0)-1]=\Delta\eta+\frac{1}{2!}(\Delta\eta)^2\Big/c_0+\frac{1}{3!}(\Delta\eta)^3\Big/c_0^2+\cdots. \tag{2.23}$$

It can be shown [17,28,29] that second-order isentropic elastic constants $C_{\alpha\beta}$ and Grüneisen constants Γ_α should be equal when the reference state is unstressed for E-based theory and e-based theory:

$$C_{\alpha\beta}=\overline{C}_{\alpha\beta}=\check{C}_{\alpha\beta},\quad \Gamma_\alpha=\overline{\Gamma}_\alpha=\check{\Gamma}_\alpha. \tag{2.24}$$

This result is consistent with the requirement that $\check{U}\approx\overline{U}$ when strains are small. Third-order isentropic constants are related, in full tensor notation, by Ref. [28]

$$\check{C}_{IJKLMN}=\overline{C}_{IJKLMN}+2\left(J_{IJKLPQ}C_{PQMN}+J_{KLMNPQ}C_{PQIJ}+J_{MNIJPQ}C_{PQKL}\right), \tag{2.25}$$

$$\begin{aligned}J_{IJKLMN}=\frac{1}{8}&\left(\delta_{IK}\delta_{JM}\delta_{LN}+\delta_{IK}\delta_{JN}\delta_{LM}+\delta_{IL}\delta_{JM}\delta_{KN}+\delta_{IL}\delta_{JN}\delta_{KM}\right.\\&\left.+\delta_{IM}\delta_{JK}\delta_{LN}+\delta_{IM}\delta_{JL}\delta_{KN}+\delta_{IN}\delta_{JK}\delta_{LM}+\delta_{IN}\delta_{JL}\delta_{KM}\right).\end{aligned} \tag{2.26}$$

Henceforward this work will use e-based theory and $\check{U}$, with (2.25) needed only to convert experimentally reported values of $\overline{C}_{\alpha\beta\gamma}$ to $\check{C}_{\alpha\beta\gamma}$.

2.2. Isotropic thermoelasticity

Thermoelastic relations simplify considerably when the solid is elastically isotropic. Hyperelastic law (2.8) reduces to the following relation between principal components of Cauchy stress σ_i and elastic principal stretch components λ_i^E [17,30]:

$$\sigma_i=\frac{1}{J^E}\lambda_i^E\frac{\partial U}{\partial\lambda_i^E}=\frac{1}{J^E}\frac{\partial U}{\partial\ln\lambda_i^E}=\frac{1}{J^E}\frac{\partial U}{\partial e_i^E}\quad(i=1,2,3). \tag{2.27}$$

Note from (2.11) that e_i^E are principal values of $\boldsymbol{e}^E$, equal to logarithmic principal stretches $\ln\lambda_i^E$. Isotropic second- and third-order elastic constants are of the following forms ($\overline{C}$ or $\check{C}$):

$$C_{IJKL}=\lambda\delta_{IJ}\delta_{KL}+\mu\left(\delta_{IK}\delta_{JL}+\delta_{IL}\delta_{JK}\right), \tag{2.28}$$

$$C_{IJKLMN} = \nu_1\left[\delta_{IJ}\delta_{KL}\delta_{MN}\right] + \nu_2\left[\delta_{IJ}(\delta_{KM}\delta_{LN}+\delta_{KN}\delta_{LM}) + \delta_{KL}(\delta_{IM}\delta_{JN} + \delta_{IN}\delta_{JM}) + \delta_{MN}(\delta_{IK}\delta_{JL}+\delta_{IL}\delta_{JK})\right] + \nu_3\left[\delta_{IK}(\delta_{JM}\delta_{LN} + \delta_{JN}\delta_{LM}) + \delta_{JL}(\delta_{IM}\delta_{KN}+\delta_{IN}\delta_{KM}) + \delta_{IL}(\delta_{JM}\delta_{KN} + \delta_{JN}\delta_{KM}) + \delta_{JK}(\delta_{IM}\delta_{LN}+\delta_{IN}\delta_{LM})\right]. \tag{2.29}$$

Second-order constants obey

$$C_{11} = \lambda+2\mu, \quad C_{12}=\lambda, \quad C_{44}=\mu; \quad \nu = \lambda/(2\lambda+2\mu), \quad K = \lambda+\frac{2}{3}\mu. \tag{2.30}$$

Shear modulus is μ, bulk modulus is K, and Poisson's ratio is ν. Third-order constants obey the following relations ($\overline{C}_{\alpha\beta\gamma}$ or $\check{C}_{\alpha\beta\gamma}$):

$$C_{111} = \nu_1+6\nu_2+8\nu_3, \quad C_{112}=\nu_1+2\nu_2, \quad C_{123}=\nu_1, \quad C_{144}=\nu_2, \quad C_{155}=\nu_2+2\nu_3, \quad C_{456}=\nu_3. \tag{2.31}$$

For isotropic materials, (2.25) reduces to

$$\check{\nu}_1 = \overline{\nu}_1, \quad \check{\nu}_2 = \overline{\nu}_2+\lambda, \quad \check{\nu}_3 = \overline{\nu}_3+\frac{3}{2}\mu. \tag{2.32}$$

For hydrostatic elastic loading ($\boldsymbol{\sigma} = -p\mathbf{1}$, $\boldsymbol{F} = J^{E1/3}\mathbf{1}$), pressure derivatives of tangent bulk modulus B and tangent shear modulus G at the reference state are [29,31,32]

$$B_0' = (\mathrm{d}B/\mathrm{d}p)\big|_{p=0} = -\frac{1}{K}\left(\overline{\nu}_1+2\overline{\nu}_2+\frac{8}{9}\overline{\nu}_3\right) = -\frac{1}{K}\left(\check{\nu}_1+2\check{\nu}_2+\frac{8}{9}\check{\nu}_3\right)+2. \tag{2.33}$$

$$G_0' = (\mathrm{d}G/\mathrm{d}p)\big|_{p=0} = -\frac{1}{K}\left(\overline{\nu}_2+\frac{4}{3}\overline{\nu}_3+\frac{1}{3}\mu\right)-1 = -\frac{1}{K}\left(\check{\nu}_2+\frac{4}{3}\check{\nu}_3-\lambda-\frac{5}{3}\mu\right)-1. \tag{2.34}$$

The above relations hold for isothermal or isentropic elastic constants, but the notation refers herein to isentropic constants, consistent with definitions in §2.1. The Grüneisen tensor is spherical for isotropic solids [8]:

$$\Gamma_{IJ} = \Gamma\delta_{IJ} = (3\alpha K/c_P)\delta_{IJ}. \tag{2.35}$$

Here, α is the linear coefficient of thermal expansion, and specific heat at constant pressure in the reference state is $c_P = c_0(1+3\alpha\Gamma\theta_0)$. Under hydrostatic elastic and isothermal loading, applying (2.27) and (2.33), the present model degenerates to the following pressure–volume equation of state:

$$p = -\partial\check{\Psi}/\partial J = -K_\theta[(\ln J)/J]\left[1-\frac{1}{2}(B_0'-2)\ln J\right], \tag{2.36}$$

where $K_\theta = Kc_0/c_P$ is the isothermal bulk modulus.

General benefits of the logarithmic finite strain theory can be explained as follows. The principal Cauchy stress-logarithmic elastic strain relations (2.27) demonstrate a particularly simple and convenient form for analysis of isotropic materials [33]. The logarithmic elastic and plastic strains resulting from a multiplicative decomposition of the deformation gradient (2.1) combine to a basic additive split of the total logarithmic strain tensor in (3.10) of §3.2, which facilitates mathematical analysis of the uniaxial shock problem [16]. Accuracy of the elastic theory for describing the response of a wide class of different materials subjected to various loading protocols (extension, compression, and shear) up to moderately large strains has been demonstrated elsewhere [33]. Finally, logarithmic equation of state (2.36)—which is derived naturally from the complete logarithmic nonlinear theory—has been shown [34] to be highly realistic in geophysics applications spanning small to very large pressures. Justification of use of the logarithmic theory (e.g., in contrast to linear elasticity) to describe titanium diboride in particular will become clear in §4 in the context of comparisons of constitutive model predictions to experimental compression data.

3. Shock compression analysis

Governing equations for planar shock loading, i.e., jump conditions, are reviewed in §3.1. Application of the present finite strain constitutive model is presented in §3.2, and the method of analytical solution is outlined in §3.3.

3.1. Governing equations

Consider a continuous cylinder of material through which a planar shock moves, in the x_1-direction, with natural velocity $\mathcal{D}$. Let superscripts + and − label quantities in the material ahead (i.e., upstream) and behind (i.e., downstream) from the shock. Let $[\![(\cdot)]\!]$ and $\langle(\cdot)\rangle$ denote the jump and average of a quantity across the shock:

$$[\![(\cdot)]\!] = (\cdot)^- - (\cdot)^+, \quad \langle(\cdot)\rangle = \frac{1}{2}\left[(\cdot)^- + (\cdot)^+\right]. \tag{3.1}$$

Let n be a unit normal vector to the planar shock, i.e., $\boldsymbol{n} = \partial\boldsymbol{x}/\partial x_1$. The only nonvanishing component of particle velocity is $v = \boldsymbol{v}\cdot\boldsymbol{n}$. The Cauchy stress component normal to the shock front is $\sigma = \boldsymbol{\sigma}:(\boldsymbol{n}\otimes\boldsymbol{n}) = \sigma_{11}$. The relative velocity of the material with respect to the shock is $v = v - \mathcal{D}$. Let $u = U/\rho_0$ denote internal energy per unit mass. Appropriate forms of the Rankine-Hugoniot conditions for conservation of mass, momentum, and energy are [16]

$$[\![\rho v]\!] = 0, \tag{3.2}$$

$$[\![\sigma]\!] - \rho v[\![v]\!] = 0, \tag{3.3}$$

$$[\![\rho v\left(u+\frac{1}{2}v^2\right) - \sigma v]\!] = 0. \tag{3.4}$$

The material need not be deformed uniaxially according to these conditions, but the shock velocity and particle velocity must both be rectilinear in the x_1-direction so that only normal traction is discontinuous. Therefore, these equations can apply for shock(s) passing through a pre-stressed material, as will be considered later. Adiabatic conditions have been assumed [16]: heat conduction is not included, leading to entropy production requirement

$$[\![\eta]\!] \geq 0. \tag{3.5}$$

The shock process is neither isentropic nor isothermal, in general. Using (3.2) and (3.3), energy conservation condition (3.4) can be rewritten as [16]

$$[\![u]\!] = \langle\sigma\rangle[\![1/\rho]\!]. \tag{3.6}$$

Assume that the upstream state and shock velocity $\mathcal{D}$ are known. The downstream state can be defined by the set of variables (v^-,ρ^-,σ^-,u^-). The Rankine-Hugoniot conditions provide three equations for determining this state; in order to fully determine the downstream state, a fourth equation must be supplied by the constitutive model for the shocked material, or one more of the

downstream variables must be known, e.g., observed from experiment (typically the particle velocity v^- in addition to $\mathfrak{D}$).

3.2. Shock compression analysis of an isotropic brittle solid

Consider a brittle material whose thermoelastic response is described by the theory in §2.2. Assume that the material may be statically, isothermally, and elastically pre-deformed prior to shock compression, with the following initial elastic deformation gradient in 3×3 matrix form:

$$\boldsymbol{F}_0^E = \begin{bmatrix} A_1 & 0 & 0 \\ 0 & A_2 & 0 \\ 0 & 0 & A_2 \end{bmatrix}. \tag{3.7}$$

This applies, for example, to a cylindrical specimen under uniform lateral pressure. Subsequently, let the specimen be subjected to uniaxial strain loading of the form $\boldsymbol{F}_1$, which in general may consist of ramp loading and/or multiple planar shocks, and may be elastic and inelastic:

$$\boldsymbol{F}_1 = \begin{bmatrix} \lambda_1 & 0 & 0 \\ 0 & 1 & 0 \\ 0 & 0 & 1 \end{bmatrix}. \tag{3.8}$$

The total deformation gradient of (2.1) is then

$$\begin{aligned} \boldsymbol{F} = \boldsymbol{F}_1\boldsymbol{F}_0^E &= \begin{bmatrix} \lambda_1 A_1 & 0 & 0 \\ 0 & A_2 & 0 \\ 0 & 0 & A_2 \end{bmatrix} = \boldsymbol{F}^E\boldsymbol{F}^D \\ &= \begin{bmatrix} \lambda_1^E & 0 & 0 \\ 0 & \lambda_2^E & 0 \\ 0 & 0 & \lambda_2^E \end{bmatrix} \begin{bmatrix} \lambda_1^D & 0 & 0 \\ 0 & \lambda_2^D & 0 \\ 0 & 0 & \lambda_2^D \end{bmatrix}. \end{aligned} \tag{3.9}$$

Since $\boldsymbol{F}$ is symmetric, $\boldsymbol{F} = \boldsymbol{U}$ (and similarly for its elastic and inelastic parts), so the total logarithmic strain reduces to the additive form

$$\ln\boldsymbol{U} = \ln\boldsymbol{F} = \ln\boldsymbol{F}^E + \ln\boldsymbol{F}^D = \boldsymbol{e}^E + \boldsymbol{e}^D. \tag{3.10}$$

Henceforth it is assumed that inelastic deformation is isochoric, corresponding primarily to mode II/III opening and sliding of micro-cracks. Inelastic volume changes associated with pore collapse and crack opening/dilatation are assumed to be offsetting. Thus, $J = J^E = \lambda_1^E(\lambda_2^E)^2$ and

$$\mathrm{tr}\boldsymbol{e}^D = \ln\left(\det\boldsymbol{F}^D\right) = 0 \Rightarrow e_2^D = -\frac{1}{2}e_1^D, \tag{3.11}$$

where $e_i^D = \ln\lambda_i^D$. Assume that A_1 and A_2 are known a priori, e.g., from a static elasticity calculation. Then (3.9)–(3.11) can be combined to give the following expressions for logarithmic elastic strain components in terms of $e_1 = \ln\lambda_1$ and a single inelastic strain component e_1^D:

$$e_1^E\left(e_1, e_1^D\right) = e_1 + \ln A_1 - e_1^D, \quad e_2^E\left(e_1, e_1^D\right) = \ln A_2 + \frac{1}{2}e_1^D. \tag{3.12}$$

Total volume change from the undeformed, unstressed state is

$$\ln J^E = \ln J = e_1 + \ln A_1 + 2\ln A_2. \tag{3.13}$$

The thermoelastic response is now addressed. Internal energy (2.16) becomes, for the present situation where all strain components are principal strains ($i,j,k = 1,2,3$):

$$\begin{aligned} U = \check{U}\left(e_i^E, \eta\right) &= \frac{1}{2}C_{ij}e_i^E e_j^E + \frac{1}{6}\check{C}_{ijk}e_i^E e_j^E e_k^E - \theta_0\Gamma\eta\ln J \\ &+ \theta_0\left(\eta + \frac{1}{2}\eta^2\Big/c_0\right) = \left(\frac{1}{2}\lambda + \mu\right)\left(e_1^E\right)^2 + (2\lambda + 2\mu)\left(e_2^E\right)^2 \\ &+ 2\lambda e_1^E e_2^E + \left(\frac{1}{6}\check{\nu}_1 + \check{\nu}_2 + \frac{4}{3}\check{\nu}_3\right)\left(e_1^E\right)^3 \\ &+ \left(\frac{4}{3}\check{\nu}_1 + 4\check{\nu}_2 + \frac{8}{3}\check{\nu}_3\right)\left(e_2^E\right)^3 + \left(\check{\nu}_1 + 2\check{\nu}_2\right) \\ &\times \left[\left(e_1^E\right)^2 e_2^E + \left(e_2^E\right)^2 e_1^E\right] - \theta_0\Gamma\eta\left(e_1^E + 2e_2^E\right) \\ &+ \theta_0\left(\eta + \frac{1}{2}\eta^2\Big/c_0\right). \end{aligned} \tag{3.14}$$

The following assumptions have been made. First, internal energy increase associated with generation of new crack surfaces is assumed to offset internal energy decrease associated with reduction in elastic moduli as damage progresses, the latter phenomenon being omitted. Therefore, dependence of U on ξ is omitted ($f = 0$). Second, in the unstressed reference state, conditions $U_0 = 0$ and $\eta_0 = 0$ are chosen, an assumption which does not affect the mechanical response that depends only on changes in U and η and not their absolute values. Third, entropic contribution (2.23) is truncated at second order. From (2.27), principal Cauchy stress components are

$$\begin{aligned} \sigma_1 = J^{-1}\Big[&(\lambda + 2\mu)e_1^E + 2\lambda e_2^E + \left(\frac{1}{2}\check{\nu}_1 + 3\check{\nu}_2 + 4\check{\nu}_3\right)\left(e_1^E\right)^2 \\ &+ \left(2\check{\nu}_1 + 2\check{\nu}_2\right)\left(e_2^E\right)^2 + \left(2\check{\nu}_1 + 4\check{\nu}_2\right)e_1^E e_2^E - \theta_0\Gamma\eta\Big], \end{aligned} \tag{3.15}$$

$$\begin{aligned} \sigma_2 = \sigma_3 &= J^{-1}\Big[\lambda e_1^E + (2\lambda + 2\mu)e_2^E + \left(\frac{1}{2}\check{\nu}_1 + \check{\nu}_2\right)\left(e_1^E\right)^2 + \left(2\check{\nu}_1 + 6\check{\nu}_2\right. \\ &\left. + 4\check{\nu}_3\right)\left(e_2^E\right)^2 + \left(2\check{\nu}_1 + 2\check{\nu}_2\right)e_1^E e_2^E - \theta_0\Gamma\eta\Big]. \end{aligned} \tag{3.16}$$

Cauchy pressure is

$$\begin{aligned} p &= -\frac{1}{3}\sigma_1 - \frac{2}{3}\sigma_2 \\ &= -J^{-1}\Big[\left(\lambda + \frac{2}{3}\mu\right)\left(e_1^E + 2e_2^E\right) + \left(\frac{1}{2}\check{\nu}_1 + \frac{5}{3}\check{\nu}_2 + \frac{4}{3}\check{\nu}_3\right)\left(e_1^E\right)^2 \\ &+ \left(2\check{\nu}_1 + \frac{14}{3}\check{\nu}_2 + \frac{8}{3}\check{\nu}_3\right)\left(e_2^E\right)^2 + \left(2\check{\nu}_1 + \frac{8}{3}\check{\nu}_2\right)e_1^E e_2^E - \theta_0\Gamma\eta\Big]. \end{aligned} \tag{3.17}$$

Let $\sigma_i' = \sigma_i + p$ denote deviatoric stress components. The following quantities are associated with shear stress:

$$\begin{aligned} \tau &= -\frac{1}{2}(\sigma_1 - \sigma_2) = -\frac{3}{4}(\sigma_1 + p) = -\frac{3}{4}\sigma_1' = \frac{2}{3}\sigma_2' = \frac{1}{2}(3J_2)^{1/2} \\ &= \frac{1}{2}\sigma_e, \end{aligned} \tag{3.18}$$

where $J_2 = 1/2[(\sigma_1')^2 + (\sigma_2')^2 + (\sigma_3')^2]$, and σ_e is the effective (Mises) stress, equal to the applied stress in a static uniaxial stress experiment. From (3.15) and (3.16),

$$\tau = -J^{-1}\left[\mu\left(e_1^E - e_2^E\right) + \left(\breve{\nu}_2 + 2\breve{\nu}_3\right)\left(e_1^E\right)^2 - \left(2\breve{\nu}_2 + 2\breve{\nu}_3\right)\left(e_2^E\right)^2 + \breve{\nu}_2 e_1^E e_2^E\right]. \tag{3.19}$$

In the present application of the general theory of §2.1 to brittle isotropic solids under planar shock compression, a rate independent constitutive relation is used to specify inelastic deformation in lieu of (2.13). A general yield criterion is

$$\tau = \frac{1}{2}Y; \quad Y = Y\left(\boldsymbol{e}^E, \eta, \xi\right), \quad \xi = \xi\left(e_1^D\right). \tag{3.20}$$

Dynamic yield strength Y can depend strongly on pressure $p(\boldsymbol{e}^E,\eta)$, as mentioned earlier an important feature of brittle ceramics that does not typically apply to ductile metals [16,17]. Internal variable ξ represents damage in the material and is assumed to increase monotonically with plastic strain until saturation (i.e., a percolation limit of micro-cracks, or pulverization). More general relations would be needed to address non-monotonic loading conditions. As a more specific example, the following strength expression $Y = Y(p_\eta)$ is considered:

$$Y = Y_0\left[1 + \chi\left(p_\eta / Y_0 - p_H / Y_0\right)^m\right], \quad p_\eta\left(e^E\right) = p - \theta_0 \Gamma \eta / J. \tag{3.21}$$

Here, explicit dependence on ξ is excluded, and strength depends on isentropic pressure p_η, which eliminates coupling with entropy to enable an exact analytical solution to the shock problem, as discussed later. Physically, this simplification corresponds to offsetting entropic pressure-shear hardening and thermal softening associated with defect kinetics. Yield stress at the HEL is $Y_0 > 0$, isentropic pressure at the HEL is p_H, and χ and m are parameters. For example, other models of pressure dependent strength of brittle materials essentially prescribed $m = 1/2$ [2] and $m = 1$ [12] .

3.3. Analytical solution

Independent solution variables are the set $(p, \tau, e_1^D, \eta, e_1)$, with $e_1 = \ln\lambda_1$ prescribed as the loading parameter. If the material is subjected to static lateral pre-stress of magnitude $\sigma_0 = -\sigma_2 = -\sigma_3$, constants A_1 and A_2 are determined from simultaneous solution of (3.15) and (3.16), with $\sigma_1 = 0$, $e_1^E \to \ln A_1$, $e_2^E \to \ln A_2$, $\eta \to 0$, and the isothermal modulus $\lambda \to \lambda_\theta = K_\theta - 2/3\mu$. Elastic strains can then be written as functions of e_1 and e_1^D using (3.12). Equations (3.17) and (3.19) can be written in the form $p = p(e_1, e_1^D, \eta)$ and $\tau = \tau(e_1, e_1^D)$, providing two independent equations. Combining (3.20) and (3.21) gives a third independent equation of the form $\tau = 1/2Y(e_1, e_1^D)$. A fourth independent equation is the energy conservation law across the shock, (3.6), which can be written

$$[\![U]\!] = \langle\sigma_1\rangle[\![J]\!] = -\langle\frac{4}{3}\tau + p\rangle[\![\lambda_1]\!]. \tag{3.22}$$

where internal energy in (3.14) can be expressed in the form $U = U(e_1, e_1^D, \eta)$.

The analytical solution proceeds as follows. Equating $\tau(e_1, e_1^D) = 1/2Y(e_1, e_1^D)$ gives a quadratic algebraic equation that can be solved for $e_1^D = e_1^D(e_1)$, and then $\tau[e_1, e_1^D(e_1)]$ and elastic strain components can all be calculated explicitly in terms of loading variable e_1. Equations (3.17) and (3.22) can then be solved simultaneously for $p(e_1)$ and $\eta(e_1)$, assuming that the upstream state is known a priori in (3.22). The resulting solutions are too lengthy to express in closed form, but they can be evaluated exactly in straighforward manner via simple iteration using a computer program. Once shear stress and pressure are computed, shock velocity $\mathfrak{D}$ and downstream particle velocity v^- can be obtained from the Hugoniot equations for mass and momentum conservation, (3.2) and (3.3), leading to

$$\mathfrak{D} = \left\{\left(\sigma^- - \sigma^+\right) / \left[\rho_0\left(\lambda_1^- - \lambda_1^+\right)\right]\right\}^{1/2}, \quad v^- = v^+ - \mathfrak{D}\left(\lambda_1^- - \lambda_1^+\right). \tag{3.23}$$

Here, ρ_0 is the mass density after possible pre-stress but prior to shock compression. For a single plastic wave, typically it is assumed that the upstream state is elastic [i.e., $(e_1^D)^+ = 0$] but has been stressed to the HEL by the elastic precursor. The upstream state is then the set of variables $(p^+, \tau^+, \eta^+, e_1^+)$, where the axial positive compressive stress at the HEL is $\sigma_H = p^+ + 4/3\tau^+$ and the corresponding strain induced by the shock is $e_H = \ln\lambda_1^+ = e_1^+$. The shock velocity and particle velocity of the elastic precursor are

$$\mathfrak{D}_E = \{\sigma_H / [\rho_0(1 - \exp(e_H))]\}^{1/2}, \quad v_E = \mathfrak{D}_E[1 - \exp(e_H)]. \tag{3.24}$$

If specific volume at the HEL (i.e., e_H) is known for an initially unstressed material, Y_0 can be determined from $\tau^+(e_H) = 1/2Y^+(e_H) = Y_0$. Effects of entropy production are typically small even for moderate elastic shocks [27,29] and can thus usually be omitted for the precursor, i.e., $\eta^+ \to \eta_0 = 0$. Temperature is

$$\theta = \partial\breve{U}/\partial\eta = \theta_0\left[1 - \Gamma\left(e_1^e + 2e_2^e\right) + \eta/c_0\right]. \tag{3.25}$$

The constitutive model framework of §2 and method of solution to the shock problem outlined above in §3, while applied specifically to titanium diboride in §4, are general enough to be potentially applicable to a large number of solids undergoing finite deformation, so long as their response can be treated as isotropic hyperelastic-plastic, with shear strength possibly depending strongly on pressure in the inelastic regime. For example, the shock response of brittle polycrystalline rocks and minerals [35], as well as other ceramics such as silicon carbide [36] that yield predominantly by micro-cracking, may be considered. The analysis could also be applied towards description of the shock response of metals whose inelasticity is governed by dislocation slip, as considered previously in Ref. [17] and for which pressure dependence of strength may be reduced or omitted. However, more sophisticated numerical techniques such as the plane wave method [37] are needed to address effects of dislocation interactions and slip rates on shock profiles.

4. Shock response of titanium diboride

Properties of titanium diboride are described in §4.1. Solutions to the shock problem are presented and discussed in §4.2.

4.1. Properties

Titanium diboride (TiB_2) is a hard crystalline ceramic whose grains have hexagonal symmetry. Average grain sizes in polycrystals have been reported to vary from approximately 5 to 50 μm, and initial densities from ≈95% to nearly 100% of theoretical density of 4.52 g/cm^3 [5,38]. Properties needed for application of the analysis and solution of §3 are listed in Table 1. Ambient density, second-order elastic constants, and thermoelastic constants are obtained directly from the literature. Poisson's ratio of this particular material

(corresponding to that manufactured by Cercom [4,5]) is $\nu = 0.049$, somewhat lower than that of other samples reported in Ref. [4].

Direct experimental measurements of third-order elastic constants of TiB_2 have apparently not been reported. However, values of B_0', G_0', and C_L' have been measured ultrasonically [38], where the first two are described by (2.33) and (2.34) and C_L' is the pressure derivative of the tangent longitudinal elastic modulus in the reference state. The latter can be related to second- and third-order elastic constants as [31,39]

$$C_L' = -\Big(3\check{\nu}_1 + 10\check{\nu}_2 + 8\check{\nu}_3 - 10\lambda - 12\mu\Big)/(3K) - (\lambda + 2\mu)/(3K) - 1. \tag{4.1}$$

Given B_0', G_0', C_L', and the second-order elastic constants, Equations (2.33), (2.34), and (4.1) cannot be solved simultaneously for all three independent third-order constants since these equations are not linearly independent. Instead, herein the experimentally reported axial stress at the HEL, σ_H, for an initially unstressed isotropic sample,

$$\sigma_H \approx -J_H^{-1}\left[C_{11}e_H + \frac{1}{2}\check{C}_{111}e_H^2\right] = -J_H^{-1}\left[(\lambda+2\mu)e_H + \left(\frac{1}{2}\check{\nu}_1 + 3\check{\nu}_2 + 4\check{\nu}_3\right)e_H^2\right], \tag{4.2}$$

with experimentally reported density ratio $\rho_0/\rho = J_H = \exp(e_H)$ is used with (2.33) and (2.34) to yield the third-order constants shown in Table 1. Explicitly, equations for third-order constants are

$$\check{\nu}_1 = 6K(G_0' + 1) - 2(3\lambda + 5\mu) + \check{C}_{111}, \tag{4.3}$$

$$\check{\nu}_2 = \frac{1}{12}\left[-3K(3B_0' + 16G_0' + 10) + 48\lambda + 80\mu - 9\check{C}_{111}\right], \tag{4.4}$$

$$\check{\nu}_3 = \frac{3}{16}\left[3K(B_0' + 4G_0' + 2) - 4(3\lambda + 5\mu) + 3\check{C}_{111}\right], \tag{4.5}$$

$$\check{C}_{111} \approx -2\left[(\lambda + 2\mu)/e_H + \sigma_H \exp(e_H)/e_H^2\right]; \tag{4.6}$$

where σ_H and e_H are taken from experiment "SNL-2" of Grady [5] on Cercom material; ultrasonic and shock data on this material are also tabulated in Ref. [4]. Equations (4.2) and (4.6) are approximate because entropy rise for the elastic process is omitted. This idealization has been shown acceptable in previous analysis of elastic shocks up to the HEL in quartz, sapphire, and diamond [29].

Table 1
Physical properties of TiB_2 ($\theta_0 = 295$ K; ρ_0 in g/cm^3; c_0 in MPa/K; K, μ, σ_H, Y_0 in GPa).

Label	Description	Value	Reference
ρ_0	ambient mass density	4.51	[4]
K	isentropic bulk modulus	193	[4]
μ	elastic shear modulus	249	[4]
Γ	Grüneisen constant	1.1	[38]
c_0	specific heat	2.76	[40]
B_0'	pressure derivative of bulk modulus	2.18	[4]
G_0'	pressure derivative of shear modulus	2.53	[38]
σ_H	HEL stress	6.0	[5]
e_H	HEL strain	−0.00965	[5]
$(Y_0)_1$	strength 2τ at HEL	6.16	[5] with Equation (4.7)
$(Y_0)_2$	strength 2τ at second yield	10.96	[5] with Equation (4.7)
χ_1	strength-pressure constant below second yield	1.0	model fit
χ_2	strength-pressure constant above second yield	0.5	model fit

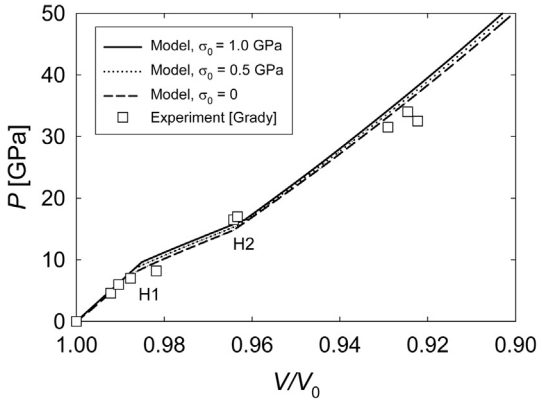

Fig. 1. Axial (Hugoniot) stress $P = -\sigma_1$: model and experiment [5]. Static lateral pre-stress is σ_0; volume after pre-stress but before shock compression is V_0.

As noted already, titanium diboride exhibits an inelastic wave structure following the elastic precursor that can be associated with two "HEL" states [5,20–22], herein labeled H1 and H2. The second is not truly an elastic limit since inelasticity, in the form of micro-cracking, commences in the material after initial yield [7,21]. A failure wave associated with lateral stress degradation has also been reported at shock pressures between first and second yield [21]. The presence of two yield points can be inferred from inflections in the particle velocity history and also is apparent from some experimental Hugoniot pressure-volume curves [5,20]. To capture the effect in the model, the pressure dependent strength equation is applied separately to regimes shocked to Hugoniot states below and above the second yield point, with different constants used in (3.21) for each regime. Let $P = -\sigma_{11} = -\sigma_1$ denote the axial stress (i.e., shock pressure), positive in compression, along the Hugoniot. Let σ_{H1} and σ_{H2} denote values of P at the first and second yield points. For titanium diboride, yield strength of (3.21) is prescribed as

$$Y = (Y_0)_1\left\{1 + \chi_1\left[p_\eta/(Y_0)_1 - p_{H1}/(Y_0)_1\right]^{1/2}\right\} \text{ for } \sigma_{H1} \le P \le \sigma_{H2};$$
$$Y = (Y_0)_2\left\{1 + \chi_2\left[p_\eta/(Y_0)_2 - p_{H2}/(Y_0)_2\right]\right\} \text{ for } P \ge \sigma_{H2}. \tag{4.7}$$

Thus, $m = 1/2$ for the response up to second yield (e.g., as in Ref. [2]), and $m = 1$ for the response beyond second yield (e.g., as in Ref. [12]). Constants $(Y_0)_1$ and $(Y_0)_2$ correspond to strength at H1 and H2; the former is constrained by $(Y_0)_1 = 2\tau(e_{H1})$, where τ is known from the nonlinear elastic solution at H1, and the value of the latter is fixed to ensure continuity of the Hugoniot stress between the two regimes at H2. Pressures p_{H1} and p_{H2} are calculated during the analysis and are not free parameters. Thus, essentially only two parameters are considered adjustable: χ_1 and χ_2. These are prescribed to fit the Hugoniot stress-volume data of [5] for initially unstressed TiB_2, as shown later in Fig. 1. Other results presented

Table 2
Error in model predictions versus experimental data [4,5] (no pre-stress).

V/V_0	Error in P [%]	Error in p [%]	Error in τ [%]
0.983	+10	−1	+12
0.971	−6	−0	−29
0.943	+1	−1	+5
0.922	+4	−1	+22
0.920	+7	−1	+29

later for mean stress, shear stress, inelastic deformation, temperature, and entropy in §4.2 (Figs. 2–4) are all predictions rather than model fits.

For samples with compressive pre-stress (i.e., $\sigma_0 > 0$), inelasticity and strength are treated as follows. Define the internal state variable associated with cumulative inelastic mechanisms (i.e., fracture and possible slip) as

$$\xi = \left|\left|\boldsymbol{e}^D\right|\right| = -\sqrt{3/2}e_1^D, \tag{4.8}$$

where (3.11) has been used. Initial yield in the pre-stressed material is defined by the condition $\tau = \frac{1}{2}Y$, where Y is given by the first of (4.7) and p_{H1} is the isentropic pressure at H1 for the material without pre-stress. Since p_η increases with compressive pre-stress at the same value of e_1, the shock stress and compressive strain associated with the shock at H1 will increase with increasing pre-stress, as shown later in §4.2. Let ξ_C be the value of ξ predicted by the model at H2 in the material without pre-stress, which corresponds to accumulation of a critical amount of damage. Second yield in the material with pre-stress is assumed to occur when $\xi \geq \xi_C$; with increasing compression beyond this point, the second of (4.7) is used for strength in the pre-stressed material. Thus, no additional fitting parameters are used to model the material with pre-stress, meaning results shown later in Fig. 5 are fully predictive.

The present analysis suggests that use of nonlinear elasticity is essential for accurate stress predictions of TiB_2 under shock compression. For the initially unstressed material at $e_1 = -0.00965$, the present nonlinear elastic model gives $P = 6.00$ GPa, $\tau = 3.08$ GPa, and $p = 1.90$ GPa. In contrast, at the same strain and

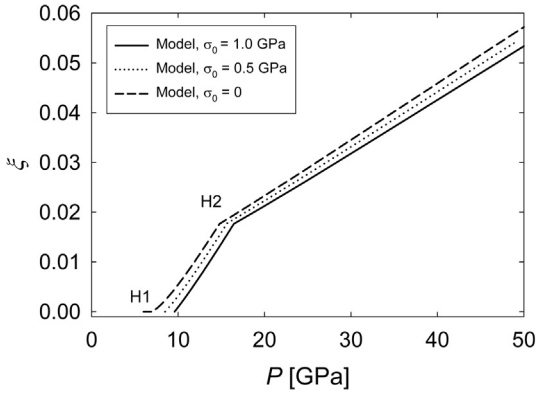

Fig. 3. Inelastic state variable $\xi = -\sqrt{3/2}e_1^D$ versus shock stress P.

with K and μ from Table 1, linear elasticity predicts $P = 5.06$ GPa, $\tau = 2.40$ GPa, and $p = 1.86$ GPa. Restricting attention now to the pressure-volume response (i.e., hydrostatic compression curve), nonlinear theory in (2.36) predicts $p = 22.5$ GPa at $V/V_0 = 0.9$, a result verified later in §4.2 as highly accurate upon comparison with experiment. In contrast, linear elasticity under-predicts the pressure as $p = K(1 - J) = 19.3$ GPa at $J = V/V_0 = 0.9$.

4.2. Results

Model results for axial stress P are compared with shock data of Grady [5] in Fig. 1. Experimental conditions correspond to no pre-

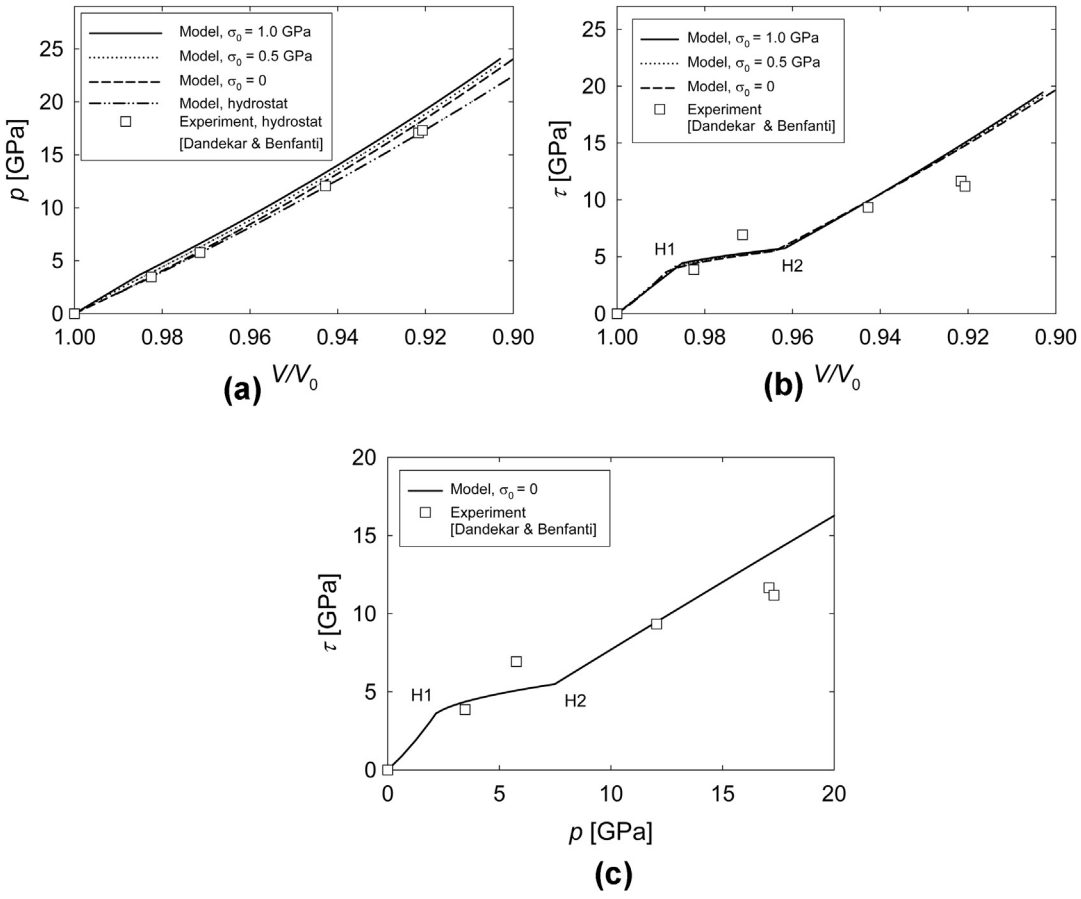

Fig. 2. Model and experiment [4]: (a) mean stress (pressure) p versus volume, (b) shear stress τ versus volume, and (c) shear stress versus mean stress.

stress ($\sigma_0 = 0$). Agreement between model and experiment is considered good, with differences between model and experiment on the order of 10% or less in Table 2. [Errors in Table 2 are computed as (predicted value minus experimental value)/(average of predicted and experimental values).] Changes in slope of P versus volume $V/V_0 = \rho_0/\rho$ are evident among the elastic regime (below H1), the first plastic regime (between H1 and H2), and the second inelastic regime (above H2). Compressive pre-stress leads to an increase in shock pressure P at the same volume ratio.

Predicted mean stress (i.e., Cauchy pressure p, positive in compression) is compared with experimental data [4] in Fig. 2(a). The upper three curves are results from shock compression, Equation (3.17). The model hydrostat is computed via (2.36), and is lower than the shock compression curve at null pre-stress primarily because the hydrostat does not include pressure rise due to entropy generation present in the shock calculation. Agreement between model and experiment is excellent, with with differences (i.e., relative error) on the order of 1% or less in Table 2. Compressive pre-stress results in a predicted increase in mean stress under shock compression. It has been suggested [5] that pore collapse may be an important source of inelasticity in titanium diboride, particularly in samples of lower initial density. Here, material of very high nominal density is considered (99.8% of theoretical density), justifying omission of the effect of porosity on compressibility.

Predicted shear stress is compared with experimental data [4] in Fig. 2(b), where the latter was determined from the offset between longitudinal stress and the hydrostat [4]. Model results are found via (3.19). Predicted trends are in reasonable agreement with the data of [4], with predicted values somewhat larger than the test data in the second inelastic regime (above H2), as is clear from Table 2. The model predicts small overall effects of pre-stress on shear stress, but τ does increase with σ_0 at large compression due to increasing p_η.

As observed in Fig. 2(c), shear stress τ increases significantly, and in a nonlinear manner, with increasing compressive pressure p. This observation emphasizes the need for inclusion of pressure dependent shear strength in constitutive modeling of polycrystalline TiB_2 applicable to the shock loading regime. A simpler model wherein yield strength Y and hence $\tau = \frac{1}{2}Y$ are constant for shocks at or exceeding the HEL, as has been assumed elsewhere as an approximation for some metals [17], would be highly inaccurate for the ceramic TiB_2.

Predicted cumulative inelastic strain ξ is shown versus shock pressure P in Fig. 3. Below H1, no inelastic deformation occurs. Between H1 and H2 (first and second yield), the increase of inelastic deformation with increasing stress is relatively rapid. Above H2, the slope of ξ versus P is less than that below H2. Inelastic deformation is reduced by compressive pre-stress.

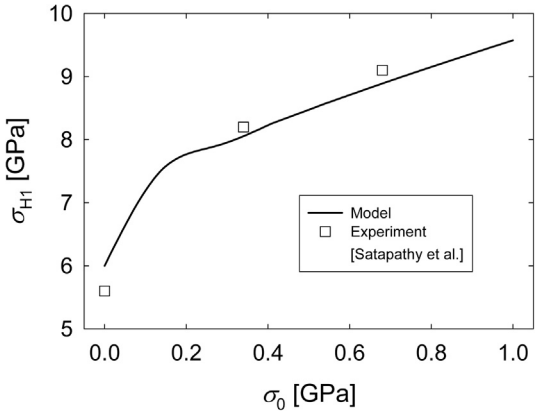

Fig. 5. Axial (Hugoniot) stress at first yield point σ_{H1} versus static lateral pre-stress σ_0: model and experiment [43].

Recovery and spall experiments [7] have demonstrated that micro-cracking, notably transgranular fracture, dominates the inelastic response at shock pressures between H1 and H2, leading to a decrease in spall strength. It has also been suggested that dislocation-based slip may be a primary inelastic mechanism above H2 [41]. Shear stress at H2, on the order of 5 GPa in Fig. 2(b), is similar in magnitude to that suggested for dislocation glide resistance in alumina [42]. Recent shock experiments on titanium diboride [43], in which compressive pre-stress was applied by shrink fitting a metal ring around a cylindrical specimen, have demonstrated an increase in spall strength with compressive pre-stress. This result is consistent with model predictions: σ_0 suppresses micro-cracking associated with ξ, leading to higher spall strength upon tensile release.

Entropy and temperature predictions are given in Fig. 4(a) and (b), respectively. Temperature rise due to the elastic precursor is approximately 3 K for titanium diboride. Slopes of entropy and temperature rise versus volume change increase with increasing compression as contributions from inelasticity and thermoelastic coupling both become large. Temperature doubles to 590 K at $V/V_0 = 0.915$ in the material without pre-stress. Pre-stress results in predicted increases in both entropy and temperature.

Fig. 5 compares model predictions of axial stress P at initial yield (σ_{H1}) with experimental data [43] at various levels of pre-stress σ_0. In these experiments on titanium diboride [43], compressive lateral pre-stress was applied by shrink fitting a metallic ring around a

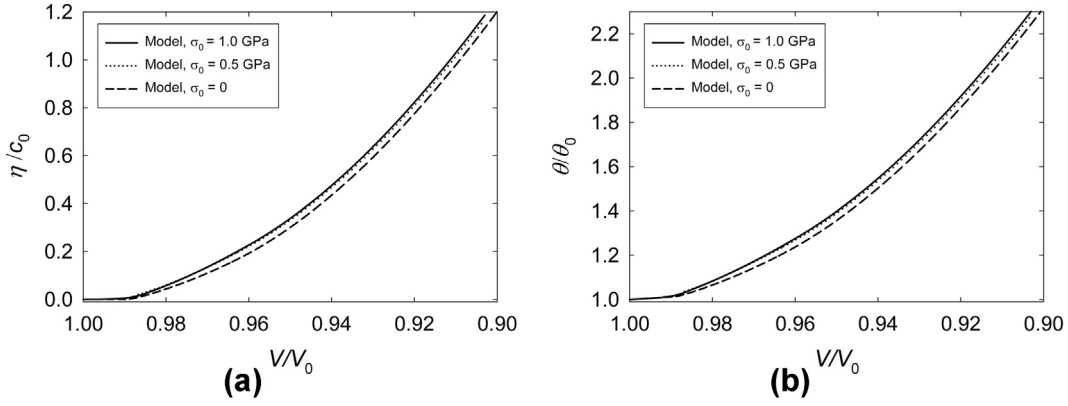

Fig. 4. Predicted (a) entropy η normalized by specific heat c_0 and (b) temperature θ normalized by initial temperature θ_0.

Table 3
Model predictions versus pre-stress σ_0.

Variable	Description	Value ($\sigma_0 = 0$)	Value ($\sigma_0 = 0.5$ GPa)	Value ($\sigma_0 = 1.0$ GPa)
ρ_0	pre-shocked mass density [g/cm^3]	4.510	4.518	4.526
σ_{H1}	initial yield (HEL) [GPa]	6.00	8.47	9.58
σ_{H2}	second yield point [GPa]	14.78	15.66	16.45
$\mathfrak{D}_E$	precursor shock velocity [km/s]	11.77	11.95	11.93
v_E	precursor particle velocity [km/s]	0.113	0.157	0.177
$\mathfrak{D}$	20 GPa shock velocity [km/s]	9.209	8.859	8.726
v^-	20 GPa particle velocity [km/s]	0.450	0.401	0.377

cylindrical ceramic specimen, as noted already. The HEL of the material without pre-stress in these experiments is 5.6 GPa, slightly lower than the model value of 6 GPa that follows from Ref. [5]. Regardless, agreement between the present model and experimental data shown in Fig. 5 is considered close, with the model predicting the correct trend and magnitude of increase in HEL with increasing pre-stress. Errors in the predicted HEL compared with experimental data (computed in the same way as in Table 2) are +7%, −1%, and −2% for pre-stress values of 0, 0.34 GPa, and 0.68 GPa, respectively.

Table 3 lists various solution variables for different levels of pre-stress. Compressive pre-stress increases both the first and second yield points and the particle velocity of the elastic precursor, the latter computed from (3.24). Pre-stress has little effect on predicted precursor wave speed. Pre-stress results in a decrease in shock velocity and particle velocity from (3.23) for a 20 GPa plastic shock. Shock velocity without pre-stress is in reasonable agreement with experiment [22].

5. Conclusions

A finite strain model has been developed for brittle solids and applied to describe shock compression of the polycrystalline ceramic titanium diboride. Analytical solutions to the planar shock problem have been obtained for material with possible lateral pre-stress. Two parameters associated with pressure dependent shear strength in regimes below and above second yield are fit to experimental Hugoniot data. The model and solution then enable prediction of mean pressure, shear stress, inelastic strain, entropy, temperature, and effects of pre-stress, all without further calibration. Results closely follow experimental observations, including an increase in the HEL and decrease in inelastic deformation with increasing compressive pre-stress.

Acknowledgment

Dr. Sikhanda Satapathy (ARL) is thanked for sharing HEL data on pre-compressed titanium diboride presented in Ref. [43] prior to publication.

References

[1] Gilman J. Electronic basis of the strength of materials. Cambridge: Cambridge Univ. Press; 2003.
[2] Rosenberg Z. On the shear strength of shock loaded brittle solids. J Appl Phys 1994;76:1543–6.
[3] Satapathy S, Dandekar D. On the source of inelasticity in ceramics. In: Swab J, editor. Advances in ceramic armor VIII. Hoboken, NJ: Wiley; 2012. pp. 31–40.
[4] Dandekar D, Benfanti D. Strength of titanium diboride under shock wave loading. J Appl Phys 1993;73:673–9.
[5] Grady D, Wise J. Dynamic properties of ceramic materials, Tech. Rep. SAND93–0610. Albuquerque NM: Sandia National Laboratories; 1993.
[6] Dandekar D. Shear strengths of aluminum nitride and titanium diboride under plane shock wave compression. J Phys IV 1994;4:379–84.
[7] Ewart L, Dandekar D. Relationship between the shock response and microstructural features of titanium diboride (Ti)B_2. In: Schmidt S, Shaner J, Samara G, Ross M, editors. Shock compression of condensed matter. New York: AIP; 1994. pp. 1201–4.
[8] Clayton J. Nonlinear mechanics of crystals. Dordrecht: Springer; 2011.
[9] Clayton J. Dynamic plasticity and fracture in high density polycrystals: constitutive modeling and numerical simulation. J Mech Phys Solids 2005;53:261–301.
[10] Clayton J. Modeling dynamic plasticity and spall fracture in high density polycrystalline alloys. Int J Solids Struct 2005;42:4613–40.
[11] Addessio F, Johnson J. A constitutive model for the dynamic response of brittle materials. J Appl Phys 1990;67:3275–86.
[12] Steinberg D. Computer studies of the dynamic strength of ceramics. J Phys III 1991;1:837–44.
[13] Curran D, Seaman L, Cooper T, Shockey D. Micromechanical model for comminution and granular flow of brittle material under high strain rate application to penetration of ceramic targets. Int J Impact Eng 1993;13:53–83.
[14] Clayton J. A model for deformation and fragmentation in crushable brittle solids. Int J Impact Eng 2008;35:269–89.
[15] Clayton J. Deformation, fracture, and fragmentation in brittle geologic solids. Int J Fract 2010;163:151–72.
[16] Germain P, Lee E. On shock waves in elastic-plastic solids. J Mech Phys Solids 1973;21:359–82.
[17] Perrin G, Delannoy-Coutris M. Analysis of plane elastic-plastic shock-waves from the fourth-order anharmonic theory. Mech Mater 1983;2:139–53.
[18] Vanderwalker D, Croft W. Dislocations in shock-loaded titanium diboride. J Mater Res 1988;3:761–3.
[19] Vanderwalker D. Fracture in titanium diboride. Phys Stat Sol A 1989;111:119–26.
[20] Fujii K, Noma T, Masamura O, Mayama T. Dynamic mechanical properties of materials measured by plate impact experiments (Si_3N_4, SiC, and TiB_2). JSME Int J A 2001;44:251–7.
[21] Bourne N, Gray G. On the failure of shocked titanium diboride. Proc R Soc Lond A 2002;458:1273–84.
[22] Zhang Y, Fukuoka K, Kikuchi M, Kodama M, Shibata K, Mashimo T. Shock compression behavior of titanium diboride. Int J Impact Eng 2005;32:643–9.
[23] Clayton J. Analysis of shock compression of strong single crystals with logarithmic thermoelastic-plastic theory. Int J Eng Sci 2014;79:1–20.
[24] Clayton J. On anholonomic deformation, geometry, and differentiation. Math Mech Solids 2012;17:702–35.
[25] Jog C. The explicit determination of the logarithm of a tensor and its derivative. J Elast 2008;93:141–8.
[26] Wallace D. Thermodynamics of crystals. New York: John Wiley & Sons; 1972.
[27] Thurston R. Waves in solids. In: Truesdell C, editor. Handbuch der Physik VIA/4. Berlin: Springer-Verlag; 1974. pp. 109–308.
[28] Dłużewski P. Anisotropic hyperelasticity based on general strain measures. J Elast 2000;60:119–29.
[29] Clayton J. Nonlinear Eulerian thermoelasticity for anisotropic crystals. J Mech Phys Solids 2013;61:1983–2014.
[30] Ogden R. Non-linear elastic deformations. Chichester: Ellis-Horwood; 1984.
[31] Guinan M, Steinberg D. Pressure and temperature derivatives of the isotropic polycrystalline shear modulus for 65 elements. J Phys Chem Solids 1974;35:1501–12.
[32] Nielsen O. Optical phonons and elasticity of diamond at megabar stresses. Phys Rev B 1986;34:5808–19.
[33] Anand L. On H. Hencky's approximate strain-energy function for moderate deformations. J Appl Mech 1979;46:78–82.
[34] Poirier J-P, Tarantola A. A logarithmic equation of state. Phys Earth Planet Inter 1998;109:1–8.
[35] Ahrens T, Gregson V. Shock compression of crustal rocks: data for quartz, calcite, and plagioclase rocks. J Geophys Res 1964;69:4839–74.
[36] Clayton J. Modeling nonlinear electromechanical behavior of shocked silicon carbide. J Appl Phys 2010;107:013520.
[37] Lloyd J, Clayton J, Austin R, McDowell D. Plane wave simulation of elastic-viscoplastic single crystals. J Mech Phys Solids 2014;69:14–32.
[38] Dodd S, Cankurtaran M, Saunders G, James B. Ultrasonic determination of the temperature and hydrostatic pressure dependences of the elastic properties of ceramic titanium diboride. J Mater Sci 2001;36:3989–96.
[39] Thurston R. Effective elastic coefficients for wave propagation in crystals under stress. J Acoust Soc Am 1965;37:348–56.
[40] Munro R. Material properties of titanium diboride. J Res Natl Inst Stand Technol 2000;105:709–20.
[41] Winkler W, Stilp A. Pressure induced macro and micromechanical phenomena in planar impacted (Ti)B_2. In: Schmidt S, Dick R, Forbes J, Tasker D, editors. Shock compression of condensed matter. New York: Elsevier; 1991. pp. 555–8.
[42] Clayton J. A continuum description of nonlinear elasticity, slip and twinning, with application to sapphire. Proc R Soc Lond A 2009;465:307–34.
[43] Satapathy S, Williams C, Dandekar D. Shock experiments to study source of inelasticity in TiB_2. In: Presented at 1st annual mach conference. MD, USA: Annapolis; April 2013.

1 (PDF) DEFENSE TECHNICAL INFORMATION CTR DTIC OCA

2 (PDF) DIRECTOR US ARMY RESEARCH LAB RDRL CIO LL IMAL HRA MAIL & RECORDS MGMT

1 (PDF) GOVT PRINTG OFC A MALHOTRA

D DANDEKAR
M GREENFIELD
R LEAVY
J LLOYD
M RAFTENBERG
S SEGLETES
A TONGE
C WILLIAMS
RDRL WMP D
R DONEY

ABERDEEN PROVING GROUND

37 (PDF) DIR USARL
RDRL CIH C
J KNAP
RDRL WM
B FORCH
J MCCAULEY
RDRL WML B
I BATYREV
B RICE
D TAYLOR
N WEINGARTEN
RDRL WML H
B SCHUSTER
RDRL WMM
J BEATTY
RDRL WMM B
G GAZONAS
D HOPKINS
B POWERS
C RANDOW
RDRL WMM E
J SWAB
RDRL WMM F
T SANO
M TSCHOPP
RDRL WMM G
J ANDZELM
RDRL WMP
S SCHOENFELD
RDRL WMP B
C HOPPEL
S SATAPATHY
M SCHEIDLER
A SOKOLOW
T WEERASOORIYA
RDRL WMP C
R BECKER
S BILYK
T BJERKE
D CASEM
J CLAYTON

INTENTIONALLY LEFT BLANK.